





# Quantitative characterization of the mass transfer of volatile amphiphiles between vapor and aqueous phases: Experiment vs theory

Ralitsa I. Uzunova<sup>a,\*</sup> , Krassimir D. Danov<sup>a,b</sup>, Rumyana D. Stanimirova<sup>a</sup>, Theodor D. Gurkov<sup>a</sup> 

<sup>a</sup> Department of Chemical & Pharmaceutical Engineering, Faculty of Chemistry & Pharmacy, Sofia University "St. Kliment Ohridski", 1164, Sofia, Bulgaria

<sup>b</sup> CoC "Smart Mechatronics, Eco- and Energy Saving Systems and Technologies", BG16RFP002-1.014-0005, Bulgaria

## ARTICLE INFO

### Keywords:

Volatile molecules  
Geraniol  
Menthol  
Vapor water exchange  
Mass transfer and adsorption  
Rate of adsorption

## ABSTRACT

The class of volatiles, which possess low saturated vapor pressures, appreciable solubilities in water, and well pronounced surface activities, have gained wide applications in diverse areas of industry, cosmetics, and medicine. One way to qualitatively characterize their mass transfer between vapor and aqueous solutions is to measure the relaxation of the interfacial tension,  $\sigma$ , with time,  $t$ , under different nonequilibrium initial conditions. This approach is applied in the present work for geraniol and menthol. By means of combining  $\sigma(t)$  data with the respective equilibrium surface tension isotherms, the instantaneous values of the fragrance adsorption,  $\Gamma(t)$ , have been determined. Quantitative characterization of the geraniol and menthol mass transfers in the case of adsorption from vapor to aqueous drops is achieved by using a mixed barrier-diffusion model. The obtained values of the rates of adsorption and desorption are compared with those reported in the literature for benzyl acetate, linalool, and citronellol. In the case of evaporation of the volatiles from their saturated aqueous solutions to the ambient atmosphere, the mass transfer is found to be driven both by mixed barrier-diffusion and by convection-enhanced mechanisms – depending on the air humidity. The quantitative description of the evaporation of volatile molecules is modelled theoretically by adsorption rate constants. In order to achieve the reported model representations, complex numerical calculations are implemented. On the other hand, having in mind the cases when one wishes to avoid extensive computational work, we developed a simple semiempirical model suitable for all five studied fragrances. This simplified approach is convenient for the express comparison and characterization of the evaporation rates. The obtained physicochemical parameters related to the evaporation and condensation of volatiles are important for the rigorous modeling of their complex mixed solutions of practical interest. The semiempirical model could be used for the quantitative classification of volatile molecules with respect to their ability to evaporate.

## 1. Introduction

The volatile organic compounds are characterized by (i) good solubility in alcohols, ethers, and some oils, and (ii) a wide range of vapor pressures at room temperature (up to tens of kPa). Thousands of volatile organic molecules have been investigated by two-dimensional gas chromatography combined with mass spectrometry [1]. While their physicochemical properties in aqueous solutions and vapors are well-studied in the literature, the available information on the adsorption and interfacial tension at liquid/vapor boundaries, evaporation and condensation rates, and the physicochemical mechanisms driving these processes, is scarce. This information is insufficient for a predictive

computer modeling of complex fluid mixtures of practical interest, involving volatile organic substances.

The change with time,  $t$ , of the short-chain-length alkane adsorption,  $\Gamma(t)$ , on (water and aqueous surfactant solution)/(saturated vapor) interfaces passes through two stages [2–12]. These volatile compounds form monolayers at initial times (up to 15 min), followed by multilayer adsorption at the later stages. The co-adsorption of the short-chain alkanes is most pronounced for the interfaces with surfactant solution concentrations below the critical micelle concentrations. The authors showed that the mechanism of alkane adsorption from vapor is barrier controlled and the adsorption rate constants for hexane and cyclohexane are of the order of  $10^{-9}$  m/s [13]. On the other hand, the fragrances have

\* Corresponding author.

E-mail address: [RU@LCPE.Uni-Sofia.BG](mailto:RU@LCPE.Uni-Sofia.BG) (R.I. Uzunova).

<https://doi.org/10.1016/j.jciso.2025.100133>

Received 13 January 2025; Received in revised form 5 March 2025; Accepted 18 March 2025

Available online 19 March 2025

2666-934X/© 2025 The Authors. Published by Elsevier B.V. This is an open access article under the CC BY-NC license (<http://creativecommons.org/licenses/by-nc/4.0/>).

low but no negligible solubility in water and for this reason, they can be adsorbed at the vapor/aqueous solution interface both from vapor and from the aqueous solution. The mass transfers from vapor to the solution and vice versa appear at nonequilibrium conditions.

The surface tension isotherms of aqueous solutions of 10 monoterpene alcohols are measured and theoretically described in Ref. [14] in order to obtain the excluded areas of adsorbed molecules, their energies of adsorption, and interaction parameters. The dynamics of adsorption of a series of volatile molecules from aqueous and surfactant solutions is found to be diffusion controlled, while that from the saturated vapor phase is mixed barrier-diffusion controlled [15–17]. It is remarkable that the adsorption rate constants from vapor for benzyl acetate, linalool, and citronellol ( $\sim 10^{-3}$  m/s) are about six orders of magnitude higher than those for hexane and cyclohexane [15]. Neutron reflectivity was used in Ref. [18]: i) to show that the volatile surfactant (linalool) can have considerable adsorption at air/solution interfaces even when there is an anionic surfactant (sodium dodecyl sulfate) which prevails in the bulk aqueous solution mixture; ii) to measure the rate of change of adsorption with time due to forced air flow over the liquid surface.

The volatile molecules have gained wide applications in diverse areas of industry, civilian, military, and national security applications [19–30]. Fragrances are an important component of home and personal care products. Even when added in low concentrations, they can change the quality of produced foams [31–33], liquid detergents [34], and emulsions [35]. The rates of release or evaporation of perfume molecules and their concentrations in mixed surfactant solutions affect the foaming behavior [36], the position and magnitude of the maximum of viscosity of solutions in the presence of salts [34,37], and the structure and dynamics of wormlike micelles [38–40].

This work is concentrated on the quantitative characterization of the geraniol and menthol adsorption and mass transfer across aqueous solution/vapor interfaces. Geraniol possesses pharmacological properties which give rise to its applications as an antioxidant [41], anti-inflammatory [42], antimicrobial [43], and antitumor [44] agent through the regulation of multiple signaling pathways in various biological processes. It can also be used to lower the total cholesterol level [45]. Menthol is an agonist of the transient receptor potential melastatin-8 channels (TRPM8) [46–48] and exerts a cooling sensation when applied to the skin and mucosal membranes [49]. It also activates the transient receptor potential cation channel, subfamily V, member 3 (TRPV3), and presents a bimodal effect in the transient receptor potential cation channel, subfamily A, member 1 (TRPA1), and the transient receptor potential cation channel, subfamily V, member 1 (TRPV1) [50–52]. The activation of TRPV3 channels contributes to wound healing in the skin and oral mucosa [53,54]. Menthol manifests antimicrobial action [55,56] against several pathogenic bacteria, antitussive action [57], and can be used in patients with mild asthma [58]. It is widely used in cosmetics, and in medicinal preparations for pain reduction [59].

In the present study, we investigate the equilibrium and dynamic properties of geraniol and menthol adsorption layers formed at the aqueous solution/vapor interfaces. The theoretical description of the experimental adsorption and surface tension isotherms (Section 3) allows us to determine the parameters of the van der Waals type adsorption model and to calculate the adsorption,  $\Gamma$ , diffusion relaxation times, and the limiting surface elasticity as a function of the interfacial tension,  $\sigma$ . The adsorption rate constants are determined by applying the mixed barrier-diffusion control model for the adsorption from vapors to aqueous drops, when the theoretically predicted  $\sigma(t)$  is fitted to the respective experimental data (Section 4). The validity of the considered model is tested on the regime of evaporation, when the saturated aqueous drop is in contact with the ambient atmosphere (where vapors of volatiles are absent). In order to avoid extensive computational work, we propose a simple semiempirical model suitable for a wide range of volatile molecules. The model is convenient for the express comparison and characterization of the volatiles evaporation rates (Section 5). The

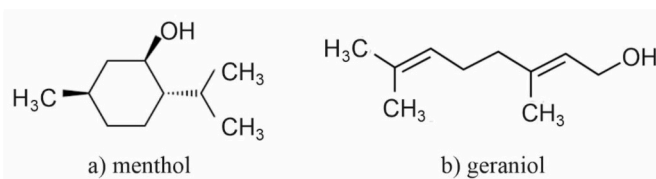


Fig. 1. Chemical structure of menthol and geraniol.

main conclusions are drawn in Section 6.

## 2. Materials and methods

### 2.1. Materials

All experiments were carried out at a temperature,  $T$ , of 25 °C. The fragrance aqueous solutions were prepared with deionized water purified by the Elix 3 water purification system (Millipore). The specific resistivity of deionized water was 18.2 M $\Omega$  cm and the viscosity was  $\eta_w = 0.889$  mPa s. The concentration of the respective fragrance in the stock aqueous solution was equal to the solubility limit,  $C_{sol}$ . The stock solution was diluted to the desired concentration  $C < C_{sol}$  and kept in a closed vessel in a thermostat at 25 °C for 24 h.

The used (–)-Menthol (menthol) was a product of TCI (>99 %, Cat. No. M0545, CAS number: 2216-51-5) with molecular mass  $M_w = 156.27$  g/mol, density  $\rho = 890$  g/dm<sup>3</sup>, and specific volume  $1/\nu_m = \rho/M_w = 5.70$  M (Fig. 1a). The solubility in water is 0.456 g/dm<sup>3</sup> and the molar solubility limit in water is  $C_{sol} = 2.92$  mM. The vapor pressure at 25 °C is  $P_{sat} = 8.49$  Pa and the corresponding saturation concentration in air is  $C_{sat} = 3.43$   $\mu$ M. The diffusion coefficient of menthol molecules in water,  $D_d = 5.97 \times 10^{-10}$  m<sup>2</sup>/s, is estimated using the Stokes-Einstein law for diffusion in simple solutions taking the equivalent spherical radius,  $r_m$ , to be equal to 4.11 Å. The diffusion coefficient of menthol vapor in air,  $D_v$ , is about  $5.9 \times 10^{-6}$  m<sup>2</sup>/s [15,60,61].

Geraniol was a product of Sigma Aldrich (>98 %, Cat. No. 163333, CAS number: 106-24-1) with molecular mass  $M_w = 154.25$  g/mol, density  $\rho = 876$  g/dm<sup>3</sup>, and specific volume  $1/\nu_m = 5.68$  M (Fig. 1b). The solubility in water is 0.686 g/dm<sup>3</sup> and the vapor pressure,  $P_{sat}$ , at 25 °C is 4.0 Pa. Thus, the geraniol molar solubility limit in water ( $C_{sol} = 4.45$  mM) is about two times higher and the saturation concentration in air ( $C_{sat} = 1.61$   $\mu$ M) is about two times lower compared to the respective values for menthol. The diffusion coefficients of geraniol molecules in water and of geraniol vapor in the air are practically the same as those for menthol. Because of the different chemical structures (Fig. 1) and the different values of concentrations  $C_{sol}$  and  $C_{sat}$ , the surface activities of menthol and geraniol are different (see Section 3).

The physicochemical parameters of a series of volatile molecules (menthol, geraniol, linalool [15], benzyl acetate [15], and citronellol [15]) are summarized in Table S1 (Appendix A). The respective values of the partition coefficient of a solute between octanol and water,  $\log P_{ow}$ , are listed in Table S1. As expected, the larger values of  $P_{ow}$  correspond to the lower solubilities of solutes in water. The only exception is menthol, which has the same  $\log P_{ow}$  as linalool, but more than 3 times lower solubility in water. All used fragrances have a pronounced adsorption at the aqueous solution/vapor interfaces so that the terms “volatile amphiphiles”, “volatile surfactants”, etc. are widely used in the literature [15–18].

### 2.2. Experimental methods and protocols

**Interfacial tension.** The dynamic surface tensions,  $\sigma(t_{age})$ , for different nominal times given by the apparatus,  $t_{age}$ , were measured using the maximum bubble pressure method (MBPM) on BP 100 automated bubble pressure tensiometer (Krüss GmbH, Germany), see Fig. S1 (Appendix A). The values of the equilibrium surface tension,  $\sigma_{eq}$ , were

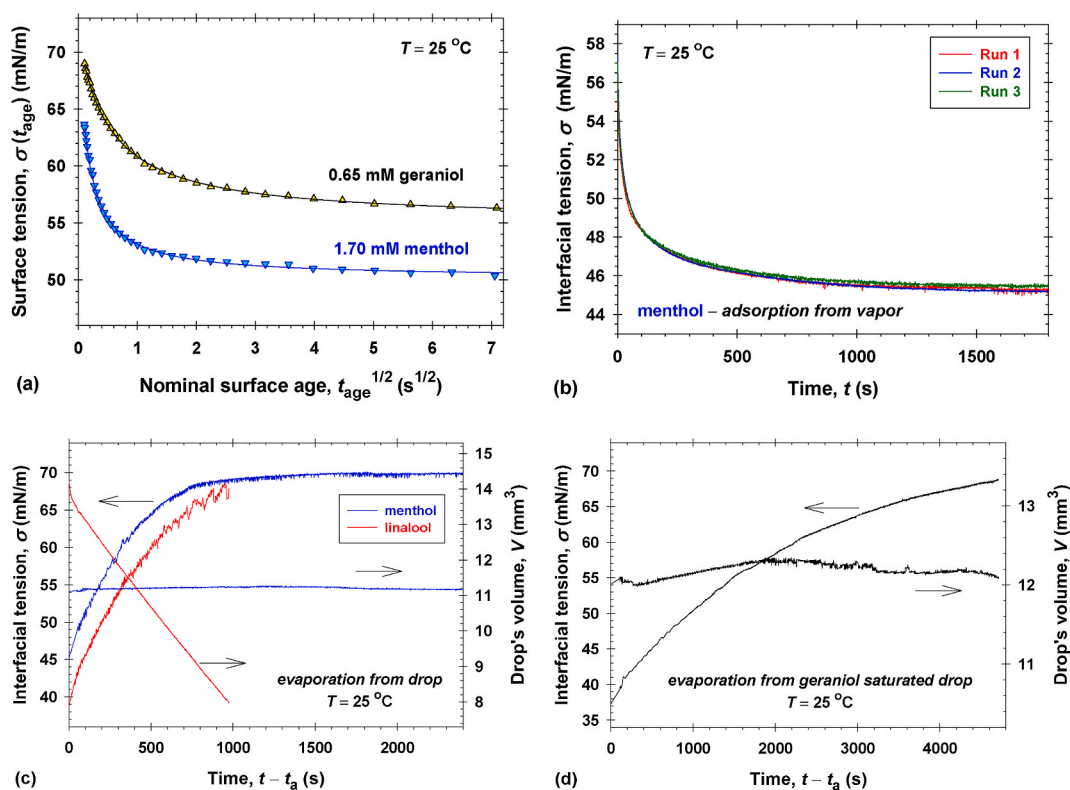


**Fig. 2.** (a) Dynamic surface tension,  $\sigma(t_{age})$ , for 1.70 mM and 0.65 mM aqueous solutions of menthol and geraniol, respectively. (b) Adsorption from menthol vapors to water drops – relaxation of the interfacial tension. (c) Comparison between the changes of the interfacial tensions and the drop's volumes in the case of an evaporation from linalool and menthol-saturated aqueous drops, red and blue curves, respectively. (d) Interfacial tension and drop's volume vs time in the case of evaporation from the geraniol-saturated aqueous drop.

calculated using the long-time-asymptotic-expansion equation, Eq. (S1) in Appendix A, which is valid for the diffusion-controlled adsorption processes [62]. The regression coefficient values of all functional interpolations were greater than 0.9995 and the precisions of the calculated equilibrium surface tensions,  $\sigma_{eq}$ , were less than 0.1 mN/m. Fig. 2a shows typical experimental data for  $\sigma(t_{age})$  – the solid lines therein represent the best fit using Eq. (S1). As expected, the two times higher concentration of menthol leads to a lower value of the equilibrium surface tension and a faster relaxation. The excellent fits shown in Fig. 2a suggest that the mechanism of adsorption from the aqueous solution is diffusion controlled.

The surface tensions at drop/vapor interfaces,  $\sigma$ , were measured using the pendant drop method (DSA 100R apparatus, Krüss GmbH, Germany). The DSA 1 software fits the drop profiles with the Laplace equation of capillarity and calculates the surface tensions with precision of 0.1 mN/m, also the drop volumes and areas, and the respective fit errors. The fit errors were small in all studied cases; therefore, the vapor/solution interfaces are fluid [63], the conventional Laplace equation of capillarity is valid, and the adsorption layers at the drop surfaces are isotropic.

**Adsorption from vapor to water drop.** In this regime, the experimental protocol is similar to that described in Ref. [15]. Pure menthol or geraniol was placed at the bottom of a cuvette that was capped with a piece of filter paper soaked with the given volatile compound. The cuvette was placed in the temperature control chamber TC 40 (Krüss GmbH, Germany) of DSA 100 R apparatus at a fixed temperature,  $T$ , of  $25^\circ\text{C}$ . A drop of deionized water was formed at the tip of a metal needle with a diameter of 1.83 mm in the saturated vapor atmosphere. The interfacial tension,  $\sigma$ , decreases with time,  $t$ , because of the adsorption of species from the vapor to the drop's surface, and  $\sigma(t)$  reaches the equilibrium value,  $\sigma_{eq}$ , after a long enough time. Three independent runs for the relaxation of the interfacial tension in the case of adsorption from

menthol vapors are included in Fig. 2b. Therein, it is seen that the reproducibility of  $\sigma(t)$  data is excellent. The experimental data for  $\sigma(t)$ , when geraniol adsorbs from its vapor to the drop's surface, are summarized in Fig. S2a (Appendix A). In all cases, the drop's areas,  $A(t)$ , were approximately constants (see Figs. S2a and S2b in Appendix A).

**Evaporation of volatile compounds from drop.** After reaching the steady-state values of the interfacial tension at a given time,  $t_a$  ( $t_a = 1800$  s for menthol, Fig. 2b, and  $t_a = 3400$  s for geraniol, Fig. S2a in Appendix A), the cuvette with fragrance vapors was removed. In our previous experiments with benzyl acetate, linalool, and citronellol [15], the respective evaporation of the volatiles from the aqueous solutions was measured for drops in contact with the ambient air atmosphere in the room. As a result, the drop's volumes decrease considerably (Fig. 2c) because of the water evaporation – the desorption of the volatile molecules from the drop's surface is affected by the water evaporation [15]. To eliminate the effect of the simultaneous water and fragrance molecules evaporation, the cuvette with menthol (geraniol) vapors was replaced by a cuvette with saturated water vapors. There was a small amount of deionized water at the bottom of the cuvette which was covered with a wet piece of filter paper. Following this procedure, the drop's volumes remain constant in all experiments, see Figs. 2c and 2d.

When the aqueous drop, which is initially saturated with volatile molecules, comes into a contact with the air in the cuvette, the desorption of the menthol (geraniol) molecules from the drop's interface leads to an exhaustion of the menthol (geraniol) concentration in the liquid phase. As a result, the interfacial tension,  $\sigma(t)$ , increases with time and  $\sigma(t)$  relaxes to a steady-state value,  $\sigma_{fin}$ . The cuvette's volume is much larger than the drop's volume but nevertheless,  $\sigma_{fin}$  does not equal the value of the pure water/air surface tension,  $\sigma_0 = 72.2$  mN/m at  $T = 25^\circ\text{C}$ . In the case of menthol,  $\sigma_{fin} = 70$  mN/m and the final concentration of the menthol vapor in the cuvette is  $0.0849 \mu\text{M}$ ; in the case of geraniol,  $\sigma_{fin} = 69$  mN/m and the final concentration of the geraniol

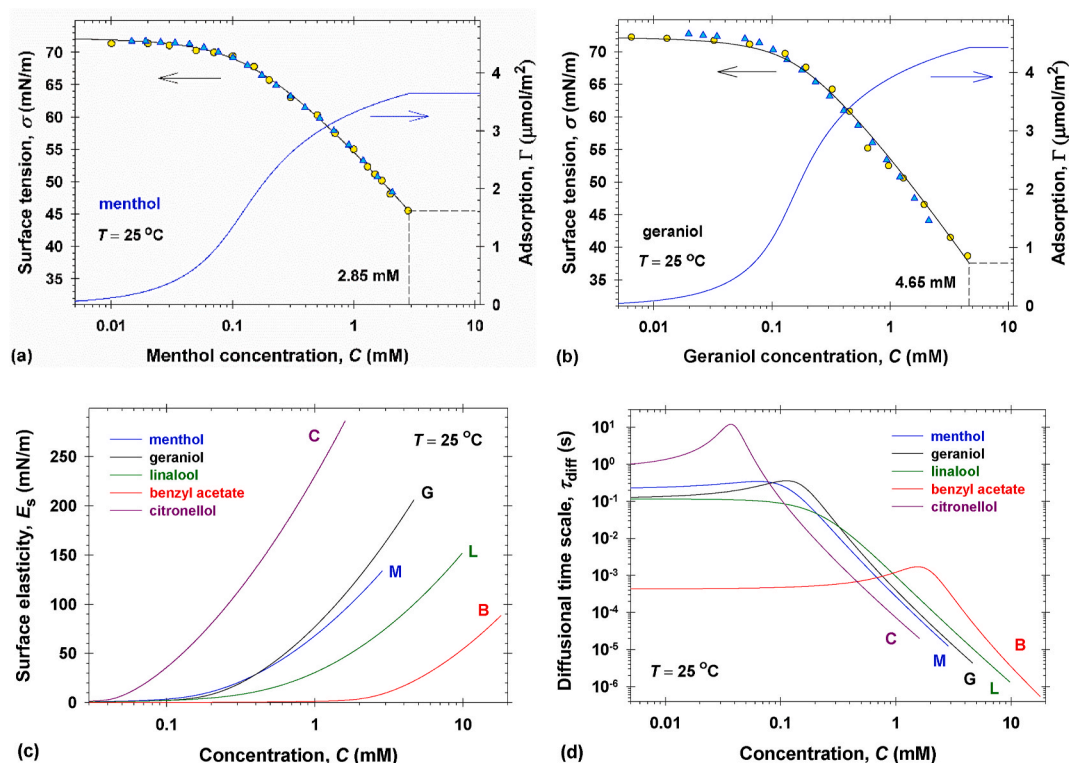


Fig. 3. Surface tension isotherms for (a) menthol and (b) geraniol aqueous solutions: o – experimental data measured at  $T = 25\text{ }^{\circ}\text{C}$  using MBPM (see Section 2.2);  $\Delta$  – experimental data measured at  $T = 20\text{ }^{\circ}\text{C}$  using the Wilhelmy plate method [14]; solid lines – the best theoretical curves for the surface tension vs concentration (left axis) and the respective calculated curves for the adsorption vs concentration (right axis). Theoretically predicted (c) surface elasticities,  $E_s$ , and (d) diffusional time scales,  $\tau_{\text{diff}}$ , vs concentrations of menthol (M), geraniol (G), linalool (L), benzyl acetate (B), and citronellol (C).

vapor in the cuvette is lower than  $0.0398\text{ }\mu\text{M}$ .

### 3. Equilibrium properties of adsorption layers

One way to characterize the evaporation and condensation rates of menthol and geraniol is to measure the change with time,  $t$ , of the subsurface fragrance concentrations in the aqueous solution,  $c_{d,s}(t)$ , in the vapor phase,  $c_{d,v}(t)$ , and the adsorption,  $\Gamma(t)$ , at the aqueous solution/vapor interface. From experimental dependencies of  $c_{d,s}$ ,  $c_{v,s}$ , and  $\Gamma$  on time, one can obtain information on the mechanism of adsorption (diffusion, barrier, or mixed barrier-diffusion controlled) and which of the bulk phases is in a quasi-equilibrium with the interfacial phase. An alternative approach is to measure the relaxation of the interfacial tension with time. For a given instantaneous value of  $\sigma(t)$ , one calculates the adsorption,  $\Gamma(t)$ , using the 2D equation of surface state,  $\sigma = \sigma(T, \Gamma)$ . Note, that the relationship  $\sigma = \sigma(T, \Gamma)$  is valid both at equilibrium and under dynamic conditions. Thus, the interfacial tension isotherms are of key importance for the study of the transfer kinetics of volatiles from vapor to aqueous drops and vice versa.

At equilibrium, the chemical potentials of the surface-active component in the bulk and interfacial phases are equal. Therefore,  $KC = \alpha f(\Gamma)\Gamma$ , where  $K$  is the equilibrium adsorption constant related to the aqueous phase,  $\alpha$  is the excluded area per molecule in the interfacial phase, and  $f(\Gamma)$  is the surface activity coefficient [14,15,64,65]. The free energy of adsorption,  $E$ , is directly related to the adsorption constant, that is  $\ln(K/v_m) = E/(k_B T)$ , where  $k_B$  is the Boltzmann constant. Postulating concrete mechanisms of adsorption, different dependencies of the surface activity coefficient on the adsorption and temperature have been obtained in the literature. In the case of non-localized adsorption model (van der Waals type of the adsorption isotherm), the expression for the surface activity coefficient reads [14,15,64,66]:

$$f(\Gamma) = \frac{1}{1 - \Gamma\alpha} \exp\left(\frac{\Gamma\alpha}{1 - \Gamma\alpha} - \frac{2\beta}{k_B T} \Gamma\right) \quad (1)$$

The non-hard-core interactions between adsorbed molecules in the lateral direction are accounted for by the interaction parameter,  $\beta$ , in Eq. (1). The two-dimensional equation of state relates the surface pressure,  $\pi_s = \sigma_0 - \sigma$ , and the adsorption,  $\Gamma$ . From the Gibbs adsorption equation,  $d\pi_s = \Gamma d(k_B T \ln C)$ , one obtains the particular form of the 2D equation of state that corresponds to Eq. (1):

$$\pi_s = k_B T \frac{\Gamma}{1 - \Gamma\alpha} - \beta \Gamma^2 \quad (2)$$

Figs. 3a and 3b show the experimental values (o symbols) of the equilibrium surface tension measured by MBPM at  $T = 25\text{ }^{\circ}\text{C}$  for different concentrations of menthol and geraniol in water, respectively. Constant values of the surface tension versus concentration are obtained for  $C > 2.85\text{ mM}$  in the case of menthol and for  $C > 4.65\text{ mM}$  in the case of geraniol aqueous solutions. Note that these threshold concentrations are close to the literature values for the respective molar solubility limits,  $C_{\text{sol}}$ , listed in Table S1 (Appendix A). Thus, the dashed vertical lines in Figs. 3a and 3b show the positions of the critical aggregation concentration. The comparison with the surface tension isotherms ( $\Delta$  symbols) of menthol and geraniol aqueous solutions measured at  $T = 20\text{ }^{\circ}\text{C}$  using the Wilhelmy plate method [14] demonstrates that the agreement is quite good. The concurrence between surface tension isotherms measured using dynamic (MBPM) and static (Wilhelmy plate) methods proves the purity of the used fragrance samples [67].

The solid lines plotted with the left axis in Figs. 3a and 3b represent the best theoretical fits using three adjustable parameters: adsorption constant  $K$ ; excluded area per molecule  $\alpha$ ; interaction parameter  $\beta$ . The obtained best fit parameters of the van der Waals isotherms for menthol and geraniol and those taken from Ref. [15] for linalool, benzyl acetate, and citronellol aqueous solutions are summarized in Table S1 (Appendix

A). It is clearly evident that the excluded area per molecule,  $\alpha$ , of menthol ( $34.6 \text{ \AA}^2$ ) is slightly lower than that of benzyl acetate ( $35.6 \text{ \AA}^2$ ). Note that the menthol chemical structure consists of a cyclohexanol ring (Fig. 1), while that of benzyl acetate – of a benzene ring (Fig. S3, Appendix A). In contrast, the excluded areas per molecule of geraniol, linalool, and citronellol are approximately equal ( $30 \text{ \AA}^2$ ). This result is in agreement with the chemical structure of the volatiles. With respect to the free energy of adsorption,  $E$ , the fragrances can be ordered from the most to the least surface active as follows: citronellol ( $9.80 k_B T$ ) > menthol ( $9.51 k_B T$ ) > geraniol ( $9.07 k_B T$ ) > linalool ( $9.05 k_B T$ ) > benzyl acetate ( $6.64 k_B T$ ). This order correlates well with the water solubilities of the volatile compounds (Table S1, Appendix A) – high  $E$  refers to low solubility limit,  $C_{\text{sol}}$ . The calculated values of the adsorptions vs concentrations are shown in Figs. 3a and 3b (the solid lines affiliated with the right axis). As it should be, the saturation adsorption of menthol ( $3.64 \text{ \mu mol/m}^2$ ) is lower than that of geraniol ( $4.42 \text{ \mu mol/m}^2$ ).

The limiting surface elasticity,  $E_s$ , is a thermodynamic property of the adsorption layer and  $E_s$  is defined as follows [64,65]:

$$E_s \equiv \frac{\partial \pi_s}{\partial \ln \Gamma} = k_B T \frac{\Gamma}{(1 - \Gamma\alpha)^2} - 2\beta \Gamma^2 \quad (3)$$

The Gibbs elasticity,  $E_{\text{Gibbs}}$ , is a dynamic property of the adsorption layer, which characterizes the dilatational elasticity at a given rate of dilatational deformation [65]. In all cases,  $E_s \geq E_{\text{Gibbs}}$  – for more details see Ref. [65]. Fig. 3c summarizes the dependencies of  $E_s$  on  $C$ , calculated from Eq. (3), for all studied volatile compounds. The highest surface elasticity pertains to the citronellol adsorption layer and the lowest one – to the benzyl acetate adsorption layer. The limiting surface elasticity,  $E_s$ , of menthol is higher than that of geraniol for  $C < 0.4 \text{ mM}$  but it becomes lower than that of the geraniol adsorption layer at higher concentrations.

The depth of aqueous solution needed to re-establish adsorption equilibrium is estimated by the characteristic adsorption length,  $h_a$ , defined by the following relationship [65]:

$$h_a \equiv \frac{\partial \Gamma}{\partial C} = k_B T \frac{\Gamma^2}{E_s C} \quad (4)$$

If the diffusion coefficient of the volatile molecules in water is  $D_d$  (see Table S1 in Appendix A), then the diffusional length,  $(D_d \tau_{\text{diff}})^{1/2}$ , is of the order of the adsorption length,  $h_a$ , whence the diffusional time scale is  $\tau_{\text{diff}} = h_a^2 / D_d$  [65]. Fig. 3d shows the calculated dependencies of  $\tau_{\text{diff}}$  on  $C$  for the studied fragrances. For low adsorptions ( $\Gamma\alpha \ll 1$ ),  $f(\Gamma) \approx 1$ ,  $h_a \approx K/\alpha$ , and the diffusional time scale is approximately constant. At large enough concentrations, the adsorption is close to the saturation adsorption (Figs. 3a and 3b), both the concentration and the limiting surface elasticity increase (Fig. 3c), and the characteristic adsorption length,  $h_a$ , decreases considerably, as shown in Eq. (4).

The obtained physicochemical parameters of the adsorption isotherms (Table S1 in Appendix A) are used in Section 4 to calculate the surface tension theoretically from the adsorption. In Section 5, the 2D equation of surface state in its implicit form,  $\Gamma = \Gamma(T, \sigma)$ , is applied to calculate the instantaneous values of the adsorption,  $\Gamma(t)$ , from the respective experimental data of the surface tension,  $\sigma(t)$ .

#### 4. Mass transfer of volatiles from vapors to aqueous drops and vice versa

*Formulation of the mixed barrier-diffusion-controlled model.* The diffusional time scales of volatile molecules in aqueous solutions,  $\tau_{\text{diff}}(s)$ , are quite short (see Fig. 3d). The values of their diffusion coefficients in the vapor phase,  $D_v$ , are four orders of magnitude larger than those in the aqueous phase,  $D_d$ , and the saturation concentrations in air,  $C_{\text{sat}}$ , are about three orders of magnitude lower than the solubility concentrations,  $C_{\text{sol}}$  (see Table S1 in Appendix A). The diffusional time scale in vapor,  $\tau_{\text{diff}}(v)$ , is estimated from the equilibrium values of the

parameters, see Eq. (4), when the ratio between the fragrance concentration in water and that in vapor is equal to the partition coefficient,  $C_{\text{sol}}/C_{\text{sat}}$ . Hence the following relationship between the diffusional time scales in vapor,  $\tau_{\text{diff}}(v)$ , and in the aqueous solution,  $\tau_{\text{diff}}(s)$ , takes place:

$$\tau_{\text{diff}}(v) = \frac{D_d C_{\text{sol}}^2}{D_v C_{\text{sat}}^2} \tau_{\text{diff}}(s) \quad (5)$$

It is shown in Table S1 (Appendix A) that  $46 < \tau_{\text{diff}}(v)/\tau_{\text{diff}}(s) < 768$  for all studied volatile molecules. Thus, the diffusional time scale in the vapor phase is considerably larger than that in the aqueous solution. Nevertheless  $\tau_{\text{diff}}(v)$  is much smaller than the characteristic experimental time scales illustrated in Figs. 2d and S2a (Appendix A). As a result: i) an intensive mass transfer of the volatiles appears in order to saturate the aqueous solution in the drop and vice versa; ii) the relaxation of the interfacial tension is considerably slower; iii) the diffusion problems in both phases (vapor and aqueous solution) must be solved simultaneously.

To simplify the numerical calculations, a spherical symmetry of the diffusion problem is considered in Ref. [15] and below. The local bulk concentration of volatile molecules in the aqueous drop solution,  $c_d(t, r)$ , and the local concentration in vapor,  $c_v(t, r)$ , depend on the time,  $t$ , and the radial coordinate,  $r$ , of the spherical coordinate system positioned in the drop center. The effective drop radius,  $a$ , is a constant (see Section 2) and from the experimental drop's volume,  $V$ , and drop's area,  $A$ , we estimate the average volume to surface value of  $a = 3V/A$ . The boundary condition of the diffusion equations written in both bulk phases, Eqs. (S2) and (S3) in Appendix A, states that the rate of change of the adsorption,  $\Gamma$ , of the volatile molecules is compensated by the diffusion fluxes from vapor,  $j_v$ , and from the aqueous phase,  $j_d$ , Eqs. (S4) and (S5) in Appendix A. To close the diffusion problem, one specifies the mechanisms of adsorption of volatile molecules from both contiguous bulk phases.

First, the experimental data illustrated in Figs. 2a and S1 (Appendix A) show that the mechanism of adsorption from the aqueous solution is diffusion controlled. Thus, the instantaneous adsorption,  $\Gamma(t)$ , is in a quasi-equilibrium with the instantaneous bulk concentration  $c_d$  at the interface,  $c_{d,s}(t) = c_d(t, a)$ , see Eq. (S6) in Appendix A. Second, the adsorption of volatile molecules from the vapor phase to the interface is slower than and/or comparable to the diffusion [15,16]. For that reason, the contiguous vapor phase is not in equilibrium with the interfacial phase and the mechanism of adsorption in the vapor phase is mixed barrier-diffusion controlled. The mass balance of fluxes in the vapor phase requires that the vapor diffusion flux,  $j_v$ , should be equal to the difference between the adsorption flux from vapor to the surface and the desorption flux from the surface to the vapor phase. From the Baret expression [66] for the non-localized adsorption (van der Waals type of isotherm), one obtains the following boundary condition [15]:

$$j_v = k_{v,\text{ads}} c_{v,s} - k_{v,\text{des}} \Gamma f(\Gamma) \quad \text{for } t > 0 \quad (6)$$

Here:  $c_{v,s}(t) = c_v(t, a)$  is the instantaneous bulk concentration  $c_v$  in the contiguous vapor phase at the place  $r = a$  which is immediately adjacent to the interface;  $k_{v,\text{ads}}$  is the adsorption rate constant;  $K_v$  is the equilibrium adsorption constant corresponding to the vapor phase,  $K_v = KC_{\text{sol}}/C_{\text{sat}}$ ;  $k_{v,\text{des}}$  is the desorption rate constant,  $k_{v,\text{des}} = ak_{v,\text{ads}}/K_v$  (the latter relationship follow from  $j_v = 0$  at equilibrium).

The concrete numerical solution of the formulated diffusion problem depends on the initial conditions, which are different in both studied cases: adsorption of volatile molecules from vapors; evaporation of fragrances from drop. The details of the numerical procedure and the respective algorithm for the numerical calculations are described in Ref. [15].

*Adsorption of volatile compounds from vapors.* In this case, the initial concentration of volatile molecules in the vapor phase,  $c_v(0, r)$  for  $r > a$ , is equal to the saturation concentration,  $C_{\text{sat}}$ . A drop of deionized water is formed (as fast as possible) in the saturated vapor atmosphere. Hence

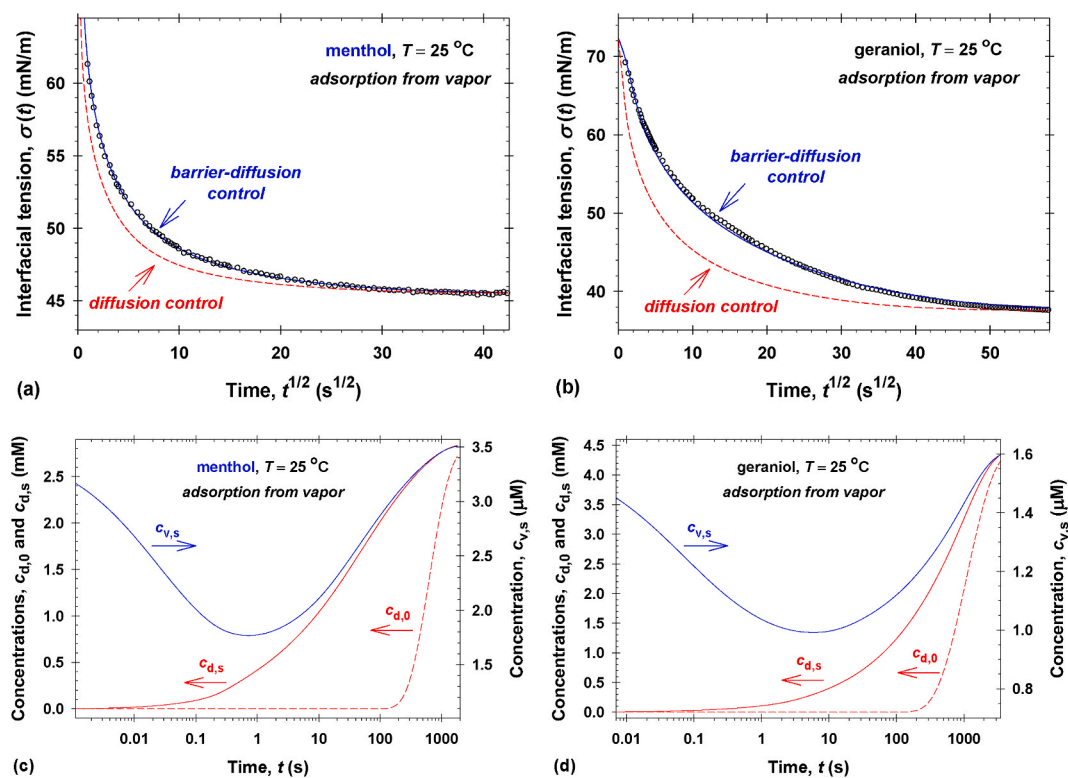


**Fig. 4.** Relaxation of the interfacial tension,  $\sigma(t)$ , in the course of adsorption from (a) menthol and (b) geraniol vapors: symbols – experimental data; dashed lines – diffusion-controlled model (no adjustable parameters); solid lines – the best theoretical fits using the mixed barrier-diffusion-controlled model (one adjustable parameter,  $k_{v,ads}$ ). Results from calculations for (c) menthol and (d) geraniol concentrations using the mixed barrier-diffusion-controlled model – dependencies of  $c_{d,0}$ ,  $c_{d,s}$ , and  $c_{v,s}$  on time.

the initial concentration in the drop,  $c_d(0,r)$  for  $r < a$ , and the initial adsorption,  $\Gamma(0)$ , are both equal to zero (see Section 2). Finally, the effective radius,  $a_c$ , of a sphere whose volume equals the cuvette's volume,  $V_c$ , is  $a_c^3 = 3V_c/(4\pi)$  and the respective boundary condition at  $r = a_c$  is  $c_v(t, a_c) = C_{sat}$ . Note that in the mixed barrier-diffusion-controlled model, all physicochemical parameters of the studied system are known (Table S1 in Appendix A) except for the adsorption rate constant,  $k_{v,ads}$ .

Figs. 4a and 4b show the experimental data (symbols) for the interfacial tension in the adsorption regime from menthol or geraniol vapors. For the sake of better illustration, the number of plotted data in Figs. 4a and 4b is reduced quite notably, see the original data presented in Figs. 2b and S2a (Appendix A). The used experimental method (DSA) gave possibility to measure the interfacial tension 1 s after the drop formation. The first experimental values for menthol and geraniol were 61.3 mN/m and 69.2 mN/m, respectively. It is obvious that the slower relaxation of  $\sigma(t)$  for geraniol allows one to make a comparison between the experiment and the theoretical predictions even for short times. In contrast, the interfacial tension in the presence of menthol vapor sharply decreases from 72.2 mN/m to 61.3 mN/m for 1 s and the experimental relaxation of  $\sigma(t)$  for the initial time interval is omitted.

The dashed lines in Figs. 4a and 4b correspond to the diffusion-controlled adsorption model, in which a quasi-equilibrium is assumed between both vapor and aqueous solution contiguous phases and the interfacial phase, so that there are no adjustable parameters. The theoretical predictions using the diffusion-controlled model deviate considerably from the experimental data. The solid lines in Figs. 4a and 4b show the best theoretical fit using the mixed barrier-diffusion-controlled adsorption model for the vapor phase, with diffusion control for the drop phase. In this model, the only adjustable parameter is the adsorption rate constant,  $k_{v,ads}$ . All experimental data are used for the data processing (5348 data points for menthol and 3355 – for geraniol), resulting in

excellent descriptions of the experimental dependencies,  $\sigma(t)$ . The obtained most probable values of  $k_{v,ads}$  are  $7.50 \pm 0.02$  mm/s for menthol and  $3.20 \pm 0.01$  mm/s for geraniol. The corresponding values of the desorption rate constants,  $k_{v,des}$ , for all studied volatile amphiphiles are summarized in Table S1 (Appendix A). The desorption time of molecules from the surface to the vapor is characterized by the value of the inverse desorption constant,  $1/k_{v,des}$ . Comparison with respect to the characteristic desorption time reveals that the citronellol, geraniol, and linalool molecules escape the surface for 15.7 s, 7.35 s, and 0.820 s, respectively. This order of volatile molecules corresponds to their surface activities (from higher to lower), surface tension isotherms, solubilities in water, and their chemical structures (see Section 3). Analogously, the menthol molecules contain cyclohexanol rings, they are less soluble in water and more surface active than the benzyl acetate molecules, which contain benzene rings. As a result, the characteristic desorption time of 1.30 s for menthol is more than 3 times longer than that for benzyl acetate (0.412 s).

The detailed diffusion model allows calculations of the subsurface concentrations,  $c_{d,s}$  and  $c_{v,s}$ , and the fragrance concentration at the drop center,  $c_{d,0}(t) = c_d(t,0)$ , as functions of time for given values of  $k_{v,ads}$  and other physicochemical parameters (Figs. 4c and 4d). As expected:  $c_{d,s} > c_{d,0}$ ; the subsurface concentration in the drop rises faster to the molar solubility limit,  $C_{sol}$ , as compared to  $c_{d,0}$ ; both  $c_{d,s}$  and  $c_{d,0}$  reach  $C_{sol}$  after sufficiently long time, and the drop's aqueous solution becomes saturated. The menthol subsurface concentration in the vapor phase,  $c_{v,s}(t)$ , initially decreases, reaching a minimum of  $c_{v,s}(t_{min}) = 0.517C_{sat}$  at  $t_{min} = 0.722$  s (Fig. 4c). In the case of geraniol (Fig. 4d), the minimum of  $c_{v,s}$  is calculated at a longer time,  $t_{min} = 5.89$  s and  $c_{v,s}(t_{min}) = 0.616C_{sat}$ , because of the more pronounced barrier mechanism of adsorption. For  $t > t_{min}$ , the subsurface concentration in the vapor phase,  $c_{v,s}$ , gradually increases over time to the value of the saturation concentration,  $C_{sat}$ . The corresponding profiles of the concentrations versus  $r$  in the drop and

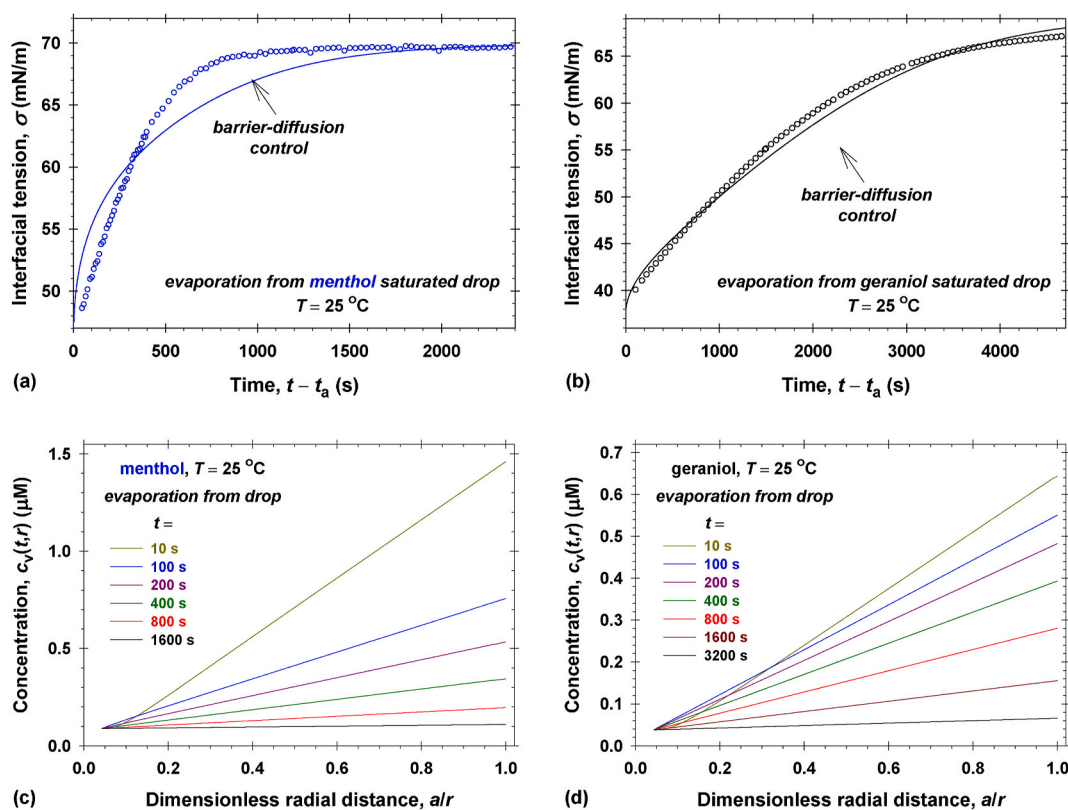


Fig. 5. Relaxation of the interfacial tension,  $\sigma(t)$ , in the regime of evaporation from (a) menthol and (b) geraniol saturated drops: symbols – experimental data; solid lines – the calculated values using the mixed barrier-diffusion-controlled model without adjustable parameters. Calculated results for (c) menthol and (d) geraniol concentration profiles in the vapor phase plotted as functions of the inverse radial distance.

vapor phases at given times are shown in Figs. S4 and S5 (Appendix A). The profiles of concentrations in both phases are not uniform and the fragrance mass transfer from vapors to the drop's aqueous solution is affected by the physicochemical properties in both phases and at the interface between them. With time, the systems become closer and closer to the equilibrium states but with considerably different time scales.

It is important to note, that the steady state values of the interfacial tensions at long times in Figs. 4a and 4b correspond exactly to the respective values of the surface tensions measured for the solubility concentrations in Figs. 3a and 3b. Thus, the systems have reached equilibrium states in which the chemical potentials of volatiles in the bulk vapor and aqueous solution phases are equal to that in the interfacial adsorption layer.

**Evaporation of volatiles from drops.** At a certain moment of time,  $t_a$ , the cuvette containing fragrance vapors is rapidly replaced by the cuvette with saturated water vapors (see Section 2). Thus, the initial conditions of the diffusion problem at  $t = t_a$  state that: i) the concentration in the aqueous solutions is  $c_d(t_a, r)$ ; ii) the adsorption is  $\Gamma(t_a)$ ; iii) the concentration in the vapor phase is low and equals the initial residual concentration,  $c_{v, \text{res}}$  (0.0849  $\mu\text{M}$  for menthol and 0.0398  $\mu\text{M}$  for geraniol). The respective boundary condition at  $r = a_c$  reads  $c_v(t_a, c) = c_{v, \text{res}}$ . The numerical calculations of the diffusion problem continue for  $t > t_a$ .

Figs. 5a and 5b show the experimental data (symbols) for the interfacial tension in the course of evaporation from drops initially containing saturated menthol or geraniol aqueous solutions. For better illustration, the number of plotted data is reduced (see Figs. 2c and 2d). The solid lines in Figs. 5a and 5b show the numerical results from the mixed barrier-diffusion-controlled model with previously determined values of the adsorption rate constants,  $k_{v, \text{ads}}$ . The theoretical prediction for menthol deviates to a certain extent from the experimental data (Fig. 5a) whereas that for geraniol accurately describes the measured

relaxation of the interfacial tension (Fig. 5b). The omitting of the possible convection fluxes in the drop leads to a deviation of the model predictions from experimental data (see Section 5).

The calculated dependencies of the subsurface concentrations,  $c_{d, s}$  and  $c_{v, s}$ , and the concentration at the drop center,  $c_{d, 0}$ , on time are summarized in Figs. S6a and S7a (Appendix A) for menthol and geraniol, respectively. Oppositely to the regime of adsorption from vapors:  $c_{d, s} < c_{d, 0}$ ; the subsurface concentration in the drop decreases faster than  $c_{d, 0}$ . The menthol subsurface concentration in the vapor phase,  $c_{v, s}(t)$ , initially increases and has a maximum of  $c_{v, s}(t_{\text{max}}) = 0.485C_{\text{sat}}$  at  $t_{\text{max}} - t_a = 0.944$  s (Fig. S6a in Appendix A). In the case of geraniol (Fig. S7a in Appendix A), the maximum of  $c_{v, s}$  is calculated at a longer time,  $t_{\text{max}} - t_a = 7.05$  s and  $c_{v, s}(t_{\text{max}}) = 0.396C_{\text{sat}}$ . For  $t > t_{\text{max}}$ , the subsurface concentration in the vapor phase,  $c_{v, s}$ , gradually decreases over time to the value of the residual concentration,  $c_{v, \text{res}}$ . The corresponding profiles of the concentrations versus  $r$  in the drop phase at given times are shown in Figs. S6b and S7b (Appendix A) for menthol and geraniol, respectively. As expected, the profile of the concentration in the drop becomes closer and closer to the uniform radial distribution of  $c_d(t, r)$ .

Figs. 5c and 5d show the calculated results for menthol and geraniol concentration profiles in the vapor phase, respectively; they are plotted as functions of the inverse radial distance. It is evident, that the dependence of  $c_v(t, r)$  is linear concerning  $1/r$  for times greater than 10 s. This linear dependence is a solution of the diffusion problem corresponding to a quasi-steady state when the term  $\partial/\partial t$  is negligible compared to the diffusion term. This conclusion is a starting point to construct the semiempirical model in Section 5.

## 5. Semiempirical model in the course of evaporation from drop

One possible "engineering" approach is proposed in Refs. [16,17] to estimate the change of  $c_{d, s}$  with time in the course of evaporation from

drop:  $c_{d,s}(t) \propto \exp(-\alpha_{mt}t)$ , where  $\alpha_{mt}$  is called “the mass transfer coefficient”. Below, we discuss the applicability of the corresponding semiempirical model, the relationship between  $\alpha_{mt}$  and the physicochemical and geometrical parameters of the studied system, and the main assumptions behind this approach.

**First assumption.** After a relatively short initial time,  $t - t_a$ , the fragrance concentration in the vapor phase becomes a solution of the steady-state diffusion problem (Figs. 5c and 5d). Thus, the radial distribution of  $c_v(t,r)$  obeys the following relationship:

$$c_v = c_{v,res} + (c_{v,s} - c_{v,res}) \left( \frac{a_c}{r} - 1 \right) \left( \frac{a_c}{a} - 1 \right)^{-1} \text{ for } t > t_a \quad (7)$$

From Eq. (7), the expression for the corresponding diffusion flux toward the vapor phase at the drop’s surface reads:

$$j_v = - \frac{D_v a_c (c_{v,s} - c_{v,res})}{a(a_c - a)} \text{ for } t > t_a \quad (8)$$

The general mass balance equation, Eq. (6), with the left-hand side substituted from Eq. (8), yields the explicit dependence of the subsurface concentration in the vapor phase,  $c_{v,s}$ , on the subsurface concentration in the aqueous phase,  $c_{d,s}$ :

$$c_{v,s} - c_{v,res} = \frac{C_{sat}}{C_{sol}} (c_{d,s} - c_{d,res}) \left[ 1 + \frac{D_v a_c}{k_{v,ads} a (a_c - a)} \right]^{-1} \text{ for } t > t_a \quad (9)$$

Here  $c_{d,res} = C_{sol} c_{v,res} / C_{sat}$  is the residual volatile molecules concentration in the drop which is in equilibrium with the vapor phase of concentration  $c_{v,res}$ .

**Second assumption.** Figs. S6b and S7b (Appendix A) show that the profiles of the fragrance concentrations in the aqueous phase,  $c_d(t,r)$ , are not uniform even after excessively long times. This was a result of the absence of convection in the drops – only the diffusion fluxes are responsible for the re-distribution of the concentration. In our experiments, the fast exchange of cuvettes (see Section 2) could lead to intensive convective fluxes inside the drop. Consequently, the aqueous solution becomes homogeneously mixed and the distribution of the fragrance concentration in the drop should be uniform, that is  $c_d(t,r) \approx c_{d,s}(t)$ . Thus, the general mass balance equation acquires a simple form – the rate of change of the total amount of the volatile molecules in the drop and at the surface,  $c_{d,s}V + \Gamma A$ , is compensated by the total mass flux from the vapor phase,  $j_v A$ . This assumption, combined with Eqs. (8) and (9), leads to the final form of the considered semiempirical model:

$$\left( 1 + \frac{3h_a}{a} \right) \frac{dc_{d,s}}{dt} = -\alpha_{mt} (c_{d,s} - c_{d,res}) \text{ for } t > t_a \quad (10)$$

Here the explicit expression for the mass transfer coefficient,  $\alpha_{mt}$ , reads:

$$\alpha_{mt} = \frac{D_v a_c}{a(a_c - a)k_{v,ads} + D_v a_c} \frac{3k_{v,ads} C_{sat}}{a C_{sol}} \quad (11)$$

The calculated values of the ratio,  $3h_a/a$ , for all studied substances and typical values of the drop’s radius,  $a = 1.5$  mm, show that  $3h_a/a \ll 1$  (Fig. S8 in Appendix A). Hence the exact solution of Eq. (10) for  $3h_a/a \ll 1$  gives the following exponential decay of the concentration in the drop solution:

$$c_{d,s}(t) = c_{d,res} + (C_{sol} - c_{d,res}) \exp[-\alpha_{mt}(t - t_a)] \text{ for } t > t_a \quad (12)$$

The following conclusions can be drawn from the obtained formula for the mass transfer coefficient, Eq. (11). The mass transfer coefficient,  $\alpha_{mt}$ , depends on: i) the physicochemical properties of the vapor phase ( $D_v$  and  $C_{sat}$ ); ii) the solubility of volatile molecules in water ( $C_{sol}$ ); iii) the mechanism of adsorption ( $k_{v,ads}$ ); iv) the geometrical configuration of the system (e.g.  $a$  and  $a_c$ ). The values of  $\alpha_{mt}$  increase with the rise of the diffusion coefficient,  $D_v$ , the saturation concentration,  $C_{sat}$ , and the adsorption rate constant,  $k_{v,ads}$ . The increase of the drop radius,  $a$ , and the molar solubility limit in water,  $C_{sol}$ , both lead to lower values of  $\alpha_{mt}$ .

The diffusion-controlled adsorption in the vapor phase is realized when  $ak_{v,ads} \gg D_v$ , so that  $\alpha_{mt}$  becomes proportional to  $1/a^2$  and independent of  $k_{v,ads}$ , see Eq. (S8) in Appendix A. If the barrier-controlled mechanism of adsorption prevails,  $ak_{v,ads} \ll D_v$ , then the values of the mass transfer coefficient are proportional to  $1/a$  and  $\alpha_{mt}$  does not depend on the diffusion coefficient in the vapor phase,  $D_v$ , see Eq. (S9) in Appendix A. Note that in our experiments, the drops’ radii are of the order of 1.5 mm and the values of  $ak_{v,ads}$  are comparable to  $D_v$ , see Table S1 (Appendix A). Thus, the mixed barrier-diffusion-controlled adsorption model is operative.

The experimental data for the interfacial tension,  $\sigma(t)$ , in the regime of evaporation from menthol and geraniol saturated drops are shown in Figs. 6a and 6b (the symbols affiliated with the left axis), respectively. From the given measured values of  $\sigma_{exp}$  and the respective surface tension isotherms, we calculated the experimental values of the adsorption,  $\Gamma_{exp}$ , they are further substituted into the adsorption isotherms,  $\Gamma(C)$ , so as to calculate the corresponding experimental values of the subsurface concentrations in the aqueous solution,  $c_{d,s}$ . These “experimental” subsurface concentrations for menthol and geraniol are plotted in Figs. 6a and 6b (the symbols affiliated with the right axis), respectively. In the case of menthol: i) the experimental effective drop’s radius during the whole process of evaporation is a constant and  $a = 1.52 \pm 0.02$  mm; ii) the calculated from Eq. (11) value of the mass transfer coefficient is  $\alpha_{mt} = 6.11 \times 10^{-3} \text{ s}^{-1}$ , see Table S1 (Appendix A). Thus, all parameters in the semiempirical formula, Eq. (12), are known and the solid line plotted in Fig. 6a (affiliated with the right axis) excellently describes the experimental data for the subsurface concentrations. The theoretically predicted values of the interfacial tension (stemming from the theoretically predicted values of  $c_{d,s}$ , and  $\Gamma$  derived therefrom) are represented by the solid line affiliated with the left axis in Fig. 6a. They practically coincide with the measured data in the range of experimental errors. In the case of geraniol, the experimental effective drop’s radius is  $a = 1.54 \pm 0.02$  mm and the calculated value of the mass transfer coefficient is approximately five times lower,  $\alpha_{mt} = 1.26 \times 10^{-3} \text{ s}^{-1}$ . The calculated theoretical dependencies of the interfacial tension and the subsurface concentration on time without using any adjustable parameter (solid lines in Fig. 6b) excellently describe the experimental data shown therein. Thus, the theoretical model based on the convection-enhanced mechanism of adsorption from water and the mixed barrier-diffusion-controlled mechanism of adsorption from the vapor phase describes the obtained experimental data during evaporation from the drop.

If both water and volatile compounds evaporate [15], the drop volume decreases with time and the effective drop radius,  $a(t)$ , becomes a function of time,  $t$ . As a result, the mass balance equation, Eq. (10), for  $3h_a/a \ll 1$  obtains the following form, see Eq. (S12) (Appendix A):

$$\frac{dc_{d,s}}{dt} = -\beta_{mt} c_{d,s} + \alpha_{mt} c_{d,res} \text{ for } t > t_a \text{ and } \beta_{mt} \equiv \alpha_{mt} + \frac{3}{a} \frac{da}{dt} \quad (13)$$

The mass transfer coefficient,  $\alpha_{mt}(t)$ , in the right-hand side of Eq. (13) depends on time, see Eq. (11), because of the dependence of the effective drop radius on time,  $a(t)$ . The experimental data for the evaporation from the linalool-saturated drop in Fig. 2c allow the calculation of the effective drop’s radius,  $a(t)$ . The experimental data for  $a(t)$  are interpolated with a high precision using a cubic polynomial, see Fig. S9 (Appendix A). As a result, one calculates the dependence of the coefficient,  $\beta_{mt}(t)$ , on time – as shown in Fig. 7b; thus, all parameters in Eq. (13) are known. The calculated solid lines in Fig. 7a (without adjustable parameters) excellently describe the experimental data for the interfacial tension (o – symbols) and the re-constructed experimental data for the subsurface concentration ( $\Delta$  – symbols). Therefore, the semiempirical approach works for both a constant value of the mass transfer coefficient,  $\alpha_{mt}$ , (see Fig. 6), and for the known dependence of the effective drop’s radius,  $a(t)$ , on time.

On the other hand, having in mind the cases when one wishes to avoid extensive computational work or when the dependence of the effective drop’s radius on time is unknown, the semiempirical model,



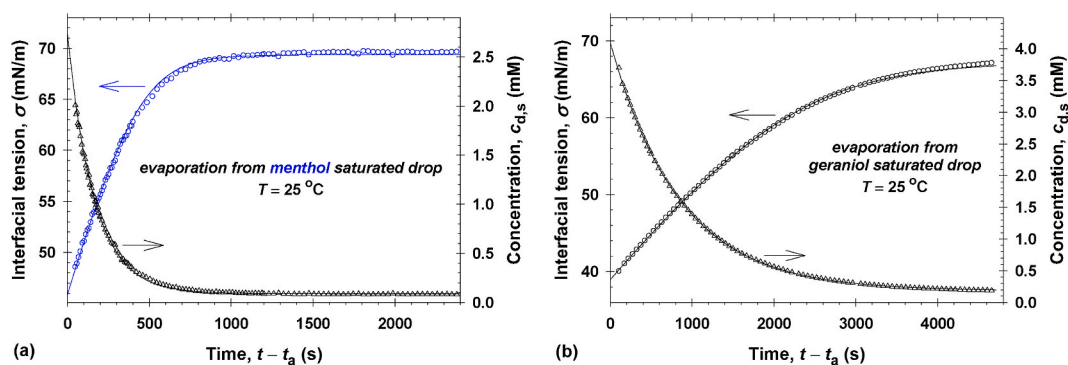


Fig. 6. Relaxation of the interfacial tension,  $\sigma(t)$ , and the subsurface concentration in the drop phase,  $c_{d,s}$ , in the regime of evaporation from (a) menthol and (b) geraniol-saturated drops:  $\circ$  – experimental data for  $\sigma(t)$ ;  $\Delta$  – experimental values of  $c_{d,s}(t)$ ; solid lines – the calculated values using the semiempirical expression for  $c_{d,s}$ , Eq. (12), and the respective 2D equation of state, Eq. (2). The “experimental” values of the concentrations,  $c_{d,s}$ , are re-constructed using the adsorption and surface tension isotherms, which are taken in the form  $\Gamma(c_{d,s})$  and  $\sigma(c_{d,s})$ , correspondingly.

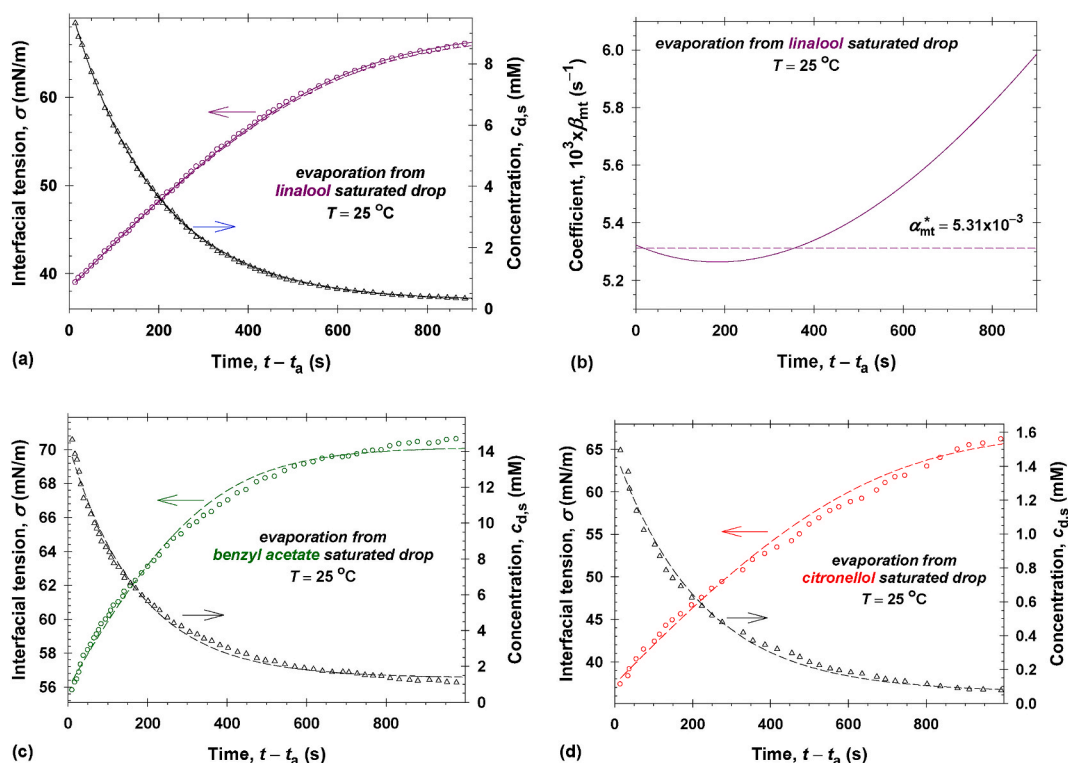


Fig. 7. Relaxation of the interfacial tension,  $\sigma(t)$ , and the subsurface concentration in the drop phase,  $c_{d,s}(t)$ , in the regime of evaporation from (a) linalool, (c) benzyl acetate, and (d) citronellol saturated drops:  $\circ$  – experimental data for  $\sigma(t)$ ;  $\Delta$  – experimental values of  $c_{d,s}(t)$ . Dashed lines – the calculated values using the semiempirical expression for  $c_{d,s}$ , Eq. (12), and the respective 2D equation of state, Eq. (2), with one (“average”) adjustable parameter,  $\alpha_{mt}^*$ . Solid lines – the calculated values using Eq. (13) without adjustable parameters. (b) Comparison between the dependence of the coefficient,  $\beta_{mt}$ , appearing in the right-hand side of Eq. (13), on time, and the mean mass transfer coefficient,  $\alpha_{mt}^*$ , for the experimental data shown in Fig. 7a.

Eq. (12), can be applied using an effective mean mass transfer coefficient,  $\alpha_{mt}^*$ . In fact,  $\alpha_{mt}^* = \alpha_{mt} = 6.11 \times 10^{-3} \text{ s}^{-1}$  for menthol (Fig. 6a) and  $\alpha_{mt}^* = \alpha_{mt} = 1.26 \times 10^{-3} \text{ s}^{-1}$  for geraniol (Fig. 6b). The processing of the experimental data for  $c_{d,s}(t)$  in Fig. 7a using Eq. (12) leads to  $\alpha_{mt}^* = 5.31 \pm 0.02 \times 10^{-3} \text{ s}^{-1}$  with a regression coefficient of 0.9999. The dashed lines in Fig. 7a show the interpolated values for the interfacial tension and the subsurface concentration. It is obvious that the description of experimental data is excellent and there are no pronounced differences between the detailed model, Eq. (13), and its simplified version, Eq. (12). The differences between the calculated interfacial tensions,  $\Delta\sigma$ , and the subsurface concentrations,  $\Delta c_{d,s}$ , from the semiempirical model, Eq. (12), using the constant mass transfer coefficient,  $\alpha_{mt}^*$ , and the

theoretical model, Eq. (13), using the time dependent mass transfer coefficient,  $\alpha_{mt}(t)$ , are shown in Fig. S10. One sees that  $\max|\Delta\sigma| < 0.4 \text{ mN/m}$  and  $\max|\Delta c_{d,s}| < 0.04 \text{ mM}$ . The comparison between the dependence of the coefficient,  $\beta_{mt}$ , appearing in the right-hand side of Eq. (13), on time, and the mean mass transfer coefficient,  $\alpha_{mt}^*$ , is shown in Fig. 7b.

The simplified approach, Eq. (12) with mean mass transfer coefficient  $\alpha_{mt}^*$ , is convenient for the express comparison and characterization of the evaporation rates. Fig. 7c shows the experimental dependencies of  $\sigma(t)$  and  $c_{d,s}(t)$  in the case of benzyl acetate [15]. The obtained result is  $\alpha_{mt}^* = 5.7 \pm 0.2 \times 10^{-3} \text{ s}^{-1}$  with a regression coefficient of 0.997. The respective data for citronellol are shown in Fig. 7d for  $\alpha_{mt}^* = 4.9 \pm 0.2 \times 10^{-3} \text{ s}^{-1}$  with a regression coefficient of 0.998. Thus, the best

interpolation lines (dashed lines in Figs. 7c and 7d) describe relatively well the experimental data, and the obtained values of  $\alpha_{\text{mt}}^*$  can be used to rank the fragrances with respect to their rates of evaporation. In a sequence from high to low rates – menthol has the highest mass transfer coefficient and the lowest value of  $\alpha_{\text{mt}}$  is obtained for geraniol.

## 6. Conclusions

Menthol and geraniol are volatile molecules, which possess low saturated vapor pressures,  $P_{\text{sat}}$ , appreciable solubilities in water, well pronounced surface activities, and have gained wide applications in pharmacy, medicine, cosmetics, and diverse areas of industry. For their controlled use, it is crucial to study not only their bulk properties in vapors and aqueous solutions, but also the adsorption at interfaces and the rate of mass transfer between their vapors and aqueous solutions. The mechanism of their mass transfer is considerably different from that of volatile organic compounds miscible with water. For example, the saturation vapor pressure of ethanol (5.9 kPa) is 1000 times higher than those pressures of geraniol and menthol; the ethanol does not form adsorption layers at the (ethanol + water) solution vapor interfaces, and the ethanol mass transfer between both phases is orders of magnitude faster [68,69].

Here, we: i) applied to menthol and geraniol our methodology [15], that was previously developed for the experimental and theoretical study of benzyl acetate, linalool, and citronellol interfacial and mass transfer properties; ii) obtained the respective physicochemical parameters and mass transfer coefficients; iii) developed a simplified approach, which is convenient for the express comparison and characterization of the evaporation rates of all five volatiles.

The general methodology consists of three main steps. *First*, the equilibrium interfacial tension isotherms are measured and processed using the van der Waals type of adsorption model. As a result, reliable values of the adsorption free energy, the excluded area per molecule, and the interaction parameter are obtained, see Section 3 and Table S1 (Appendix A). The excluded area per molecule of menthol ( $34.6 \text{ \AA}^2$ ) is lower than that of benzyl acetate ( $35.6 \text{ \AA}^2$ ), which may be attributed to the difference in their chemical structures: menthol consists of a cyclohexanol ring, while benzyl acetate contains a benzene ring. Geraniol, linalool, and citronellol have approximately equal values of  $\alpha$  ( $30 \text{ \AA}^2$ ). The volatiles can be ordered from the most to the least surface-active ones according to their energies of adsorptions as follows: citronellol ( $9.80 k_B T$ ) > menthol ( $9.51 k_B T$ ) > geraniol ( $9.07 k_B T$ ) > linalool ( $9.05 k_B T$ ) > benzyl acetate ( $6.64 k_B T$ ). This order correlates with the water solubilities of the fragrances,  $C_{\text{sol}}$  (high  $E$  matches low solubility). The thermodynamic limiting surface elasticity of the citronellol adsorption layer is the highest, while that of the benzyl acetate adsorption layer is the lowest (Fig. 3c). The diffusional time scales in the aqueous solutions of all studied volatile molecules are low (Fig. 3d), while those in the vapor phases are from 46 to 768 times higher, see Eq. (5) and Table S1 (Appendix A).

*Second*, small millimeter-sized water drops are formed in the fragrance saturated vapor and the relaxation of the interfacial tension,  $\sigma(t)$ , is measured to characterize the dynamics of adsorption and the mass transfer from vapor to the aqueous solution. In the aqueous phase, the diffusional time scale related to adsorption is much shorter than the characteristic bulk diffusion time. Thus: i) the mechanism of adsorption in the aqueous phase is diffusion controlled; ii) from the instantaneous experimental values of  $\sigma(t)$  and the respective 2D equation of state and adsorption isotherm, the instantaneous values of the adsorbed amount,  $\Gamma(t)$ , and of the subsurface concentration in the aqueous phase,  $c_{\text{d,s}}(t)$ , can be re-constructed. In contrast, the diffusional time scale in the vapor phase is comparable to the characteristic bulk diffusion time in vapor. As a result, the mechanism of adsorption from vapor is mixed barrier-diffusion controlled. The Baret expression for the non-localized adsorption [66] gives the adsorption and desorption fluxes in the

vapor phase and the adsorption rate constant in the vapor phase,  $k_{\text{v,ads}}$ , see Eq. (6). The experimental data for  $\sigma(t)$  are processed using the numerical solution of the diffusion problem to obtain the most probable value of the single unknown parameter,  $k_{\text{v,ads}}$ . The excellent theoretical descriptions of the experimental data for menthol and geraniol (Figs. 4a and 4b) and for benzyl acetate, linalool, and citronellol [15] prove the validity of the proposed model for the mechanism of adsorption and the possible classification of the volatile amphiphiles according to their adsorption rate constants,  $k_{\text{v,ads}}$ .

*Third*, aqueous drops saturated with given volatiles are placed in contact with saturated water vapor to prevent water evaporation and to keep the drop volume constant (Figs. 2c and 2d). The mass transfer of the solute from the aqueous solution to the vapor phase leads to increase of the measured interfacial tension,  $\sigma(t)$ . All interfacial physicochemical parameters to model are completely determined from the first two steps. The qualitative agreement between the theoretical model and the experimental data (Figs. 5a and 5b) suggests looking for other possible factors affecting the diffusion process in the drop phase. It is quite plausible to assume that the rapid exchange in the external conditions for the drop phase (just after the saturation stage) gives rise to intensive convective fluxes in the drop. The mechanism of diffusion in the drop switches to enhanced-convective diffusion (Figs. 6a and 6b).

After a short initial time in the evaporation regime, the dependence of the concentration in the vapor phase on the radial distance becomes close to the steady-state distribution (Figs. 5c and 5d). Assuming an enhanced-convection diffusion in the drop, we derived a semiempirical model for the mass transfer, which predicts an exponential decay of the fragrance concentration in the drop with time, Eq. (12). The analytical expression, Eq. (11), for the introduces “mass transfer coefficient”,  $\alpha_{\text{mt}}$ , shows that  $\alpha_{\text{mt}}$  depends on both physicochemical properties ( $P_{\text{sat}}$ ,  $D_{\text{v}}$ ,  $C_{\text{sol}}$ , and  $k_{\text{v,ads}}$ ) and geometrical characteristics of the system. This simple approach excellently describes experimental data both without water evaporation – for constant values of drop radii (Figs. 6a and 6b), and for known dependences of drop radii on time (Fig. 7a). The semiempirical model is also suitable for express characterization of the fragrance mass transfer using a constant mean value of  $\alpha_{\text{mt}}$  (Figs. 7c and 7d). All reliable values of the obtained physicochemical parameters are summarized in Table S1 (Appendix A), and they can be used for rigorous numerical modeling of the evaporation/condensation of complex fluids containing volatile amphiphiles as components.

## CRedit authorship contribution statement

**Ralitsa I. Uzunova:** Investigation, Formal analysis, Data curation. **Krassimir D. Danov:** Supervision, Software, Formal analysis. **Rumyana D. Stanimirova:** Investigation, Formal analysis, Data curation. **Theodor D. Gurkov:** Writing – original draft, Supervision, Methodology, Conceptualization.

## Declaration of competing interest

The authors declare the following financial interests/personal relationships which may be considered as potential competing interests: Ralitsa I. Uzunova reports financial support was provided by Department of Chemical & Pharmaceutical Engineering, Faculty of Chemistry & Pharmacy, Sofia University, 1164 Sofia, Bulgaria. Ralitsa I. Uzunova reports a relationship with Sofia University St Kliment Ohridski that includes: travel reimbursement. If there are other authors, they declare that they have no known competing financial interests or personal relationships that could have appeared to influence the work reported in this paper.

## Acknowledgements

The authors are grateful for the financial support from the Project # KP-06-H79/4-05.12.2023, with the National science fund of Bulgaria

(abbreviated as BG FNI – MON). This research was funded by the European Regional Development Fund under the Operational Program “Scientific Research, Innovation and Digitization for Smart Transformation 2021–2027”, Project CoC “Smart Mechatronics, Eco- and Energy Saving Systems and Technologies”, BG16RFPR002-1.014–0005.

## Appendix A. Supplementary data

Supplementary data to this article can be found online at <https://doi.org/10.1016/j.jciso.2025.100133>.

## Data availability

Data will be made available on request.

## References

- [1] R.A. Shellie, Volatile components of plants, essential oils, and fragrances, in: L. Ramos (Ed.), *Comprehensive Analytical Chemistry*, vol. 55, Elsevier, Amsterdam, 2009, pp. 189–213, [https://doi.org/10.1016/S0166-526X\(09\)05509-3](https://doi.org/10.1016/S0166-526X(09)05509-3).
- [2] A. Javadi, N. Moradi, H. Möwald, R. Miller, Adsorption of alkanes from the vapor phase on water drops measured by drop profile analysis tensiometry, *Soft Matter* 6 (2010) 4710–4714, <https://doi.org/10.1039/C0SM00367K>.
- [3] V.B. Fainerman, E.V. Aksenenko, V.I. Kovalchuk, A. Javadi, R. Miller, Study of the co-adsorption of hexane from the gas phase at the surface of aqueous  $C_{10}EO_8$  drops, *Soft Matter* 7 (2011) 7860–7865, <https://doi.org/10.1039/C1SM05349C>.
- [4] A. Javadi, N. Moradi, V.B. Fainerman, H. Möwald, R. Miller, Alkane vapor and surfactants co-adsorption on aqueous solution interfaces, *Colloids Surf., A* 391 (2011) 19–24, <https://doi.org/10.1016/j.colsurfa.2011.08.002>.
- [5] N. Mucic, N. Moradi, A. Javadi, E.V. Aksenenko, V.B. Fainerman, R. Miller, Mixed adsorption layers at the aqueous  $C_{12}TAB$  solution/hexane vapor interface, *Colloids Surf., A* 442 (2014) 50–55, <https://doi.org/10.1016/j.colsurfa.2013.09.019>.
- [6] N. Mucic, N. Moradi, A. Javadi, E.V. Aksenenko, V.B. Fainerman, R. Miller, Effect of partial vapor pressure on the co-adsorption of surfactants and hexane at the water/hexane vapor interface, *Colloids Surf., A* 480 (2015) 79–84, <https://doi.org/10.1016/j.colsurfa.2015.01.003>.
- [7] V.D. Mys, V.B. Fainerman, A.V. Makievski, M.P. Krafft, R. Miller, Dynamic surface tension of  $C_{10}EO_8$  at the aqueous solution/hexane vapor interface as measured by bubble pressure tensiometry, *Colloids Surf., A* 483 (2015) 137–141, <https://doi.org/10.1016/j.colsurfa.2015.06.015>.
- [8] V.B. Fainerman, E.V. Aksenenko, V. Kovalchuk, R. Miller, Surface tension of water and  $C_{10}EO_8$  solutions at the interface to hexane vapor saturated air, *Colloids Surf., A* 505 (2016) 118–123, <https://doi.org/10.1016/j.colsurfa.2016.01.043>.
- [9] T. Kairaliyeva, V.B. Fainerman, A.V. Aksenenko, V.I. Kovalchuk, Yu. Tarasevich, R. Miller, Adsorption of alkane vapor at water drop surfaces, *Colloids Surf., A* 532 (2017) 541–547, <https://doi.org/10.1016/j.colsurfa.2017.04.002>.
- [10] R. Miller, E.V. Aksenenko, V.I. Kovalchuk, D.V. Trukhin, Yu. Tarasevich, V. B. Fainerman, Mixed protein/hexane adsorption layers formed at the surface of protein solution drops surrounded by hexane vapor, *Adv. Mater. Interfac.* 4 (2017) 1600031, <https://doi.org/10.1002/admi.201600031>.
- [11] R. Miller, E.V. Aksenenko, V.I. Kovalchuk, V.B. Fainerman, Adsorption of  $C_{14}EO_8$  at the interface between its aqueous solution drop and air saturated by different alkanes vapor, *Phys. Chem. Chem. Phys.* 19 (2017) 2193–2200, <https://doi.org/10.1039/C6CP07705F>.
- [12] V.B. Fainerman, A.V. Aksenenko, S.V. Lylyk, Yu. Tarasevich, R. Miller, Adsorption of surfactants and proteins at the interface between their aqueous solution drop and air saturated by hexane vapor, *Colloids Surf., A* 521 (2017) 211–220, <https://doi.org/10.1016/j.colsurfa.2016.08.053>.
- [13] R. Miller, E.V. Aksenenko, V.I. Kovalchuk, Yu. Tarasevich, V.B. Fainerman, Adsorption of hexane and cyclohexane vapors at the water drop surface, *Physicochem. Probl. Miner. Process.* 54 (2018) 54–62, <https://www.journalsystem.com/ppmp/Adsorption-of-hexane-and-cyclohexane-vapours-at-the-water-drop-surface.75753,0,2.html>.
- [14] A. Lewandowski, K. Szymczyk, Adsorption of monoterpene alcohols at the water-air interface, *Adsorption* 25 (2019) 301–308, <https://doi.org/10.1007/s10450-019-00010-y>.
- [15] K.D. Danov, T.D. Gurkov, R.D. Stanimirova, R.I. Uzunova, Kinetics of transfer of volatile amphiphiles (fragrances) from vapors to aqueous drops and vice versa: interplay of diffusion and barrier mechanisms, *Colloids Surf., A* 625 (2021) 126931, <https://doi.org/10.1016/j.colsurfa.2021.126931>.
- [16] L.A. Tsarkova, T.D. Gurkov, Volatile surfactants: characterization and areas of application, *Curr. Opin. Colloid Interface Sci.* 60 (2022) 101592, <https://doi.org/10.1016/j.cocis.2022.101592>.
- [17] O.A. Soboleva, T.D. Gurkov, R.D. Stanimirova, P.V. Protchenko, L.A. Tsarkova, Volatile aroma surfactants: the evaluation of the adsorption–evaporation behavior under dynamic and equilibrium conditions, *Langmuir* 38 (2022) 2793–2803, <https://doi.org/10.1021/acs.langmuir.1c02871>.
- [18] J. Penfold, R.K. Thomas, R. Bradbury, I. Tucker, J.T. Petkov, C.W. Jones, J.R. P. Webster, Probing the surface of aqueous surfactant–perfume mixed solutions during perfume evaporation, *Colloids Surf., A* 520 (2017) 178–183, <https://doi.org/10.1016/j.colsurfa.2017.01.082>.
- [19] W. Jia, H.-H. Qiu, Experimental investigation of droplet dynamics and heat transfer in spray cooling, *Exp. Therm. Fluid Sci.* 27 (2003) 829–838, [https://doi.org/10.1016/S0894-1777\(03\)00015-3](https://doi.org/10.1016/S0894-1777(03)00015-3).
- [20] Z. Lin, S. Granick, Patterns formed by droplet evaporation from a restricted geometry, *J. Am. Chem. Soc.* 127 (2005) 2816–2817, <https://doi.org/10.1021/ja044792z>.
- [21] J. Kim, Spray cooling heat transfer: the state of the art, *Int. J. Heat Fluid Flow* 28 (2007) 753–767, <https://doi.org/10.1016/j.ijheatfluidflow.2006.09.003>.
- [22] N. Kumari, S.V. Garimella, Characterization of the heat transfer accompanying electrowetting or gravity-induced droplet motion, *Int. J. Heat Mass Tran.* 54 (2011) 4037–4050, <https://doi.org/10.1016/j.ijheatmasstransfer.2011.04.015>.
- [23] J. Tissot, P. Boulet, F. Trinquet, L. Fournaison, H. Macchi-Tejeda, Air cooling by evaporating droplets in the upward flow of a condenser, *Int. J. Therm. Sci.* 50 (2011) 2122–2131, <https://doi.org/10.1016/j.ijthermalsci.2011.06.004>.
- [24] A. Ebrahimi, P. Dak, E. Salm, S. Dash, S.V. Garimella, R. Bashir, M.A. Alam, Nanotextured superhydrophobic electrodes enable detection of attomolar-scale DNA concentration within a droplet by non-faradaic impedance spectroscopy, *Lab Chip* 13 (2013) 4248–4256, <https://doi.org/10.1039/C3LC50517K>.
- [25] L. Zhang, J. Wu, M.N. Hedhili, X. Yang, P. Wang, Inkjet printing for direct micropatterning of a superhydrophobic surface: toward biomimetic fog harvesting surfaces, *J. Mater. Chem. A* 3 (2015) 2844–2852, <https://doi.org/10.1039/C4TA05862C>.
- [26] J. Sun, B. Bao, J. Jiang, M. He, X. Zhang, Y. Song, Facile fabrication of a superhydrophilic-superhydrophobic patterned surface by inkjet printing a sacrificial layer on a superhydrophilic surface, *RSC Adv.* 6 (2016) 31470–31475, <https://doi.org/10.1039/C6RA02170K>.
- [27] H. Kim, F. Boulogne, E. Um, I. Jacobi, E. Button, H.A. Stone, Controlled uniform coating from the interplay of Marangoni flows and surface-adsorbed macromolecules, *Phys. Rev. Lett.* 116 (2016) 124501, <https://doi.org/10.1103/PhysRevLett.116.124501>.
- [28] MdA. Mahmud, B.D. MacDonald, Experimental investigation of interfacial energy transport in an evaporating sessile droplet for evaporative cooling applications, *Phys. Rev. E* 95 (2017) 012609, <https://doi.org/10.1103/PhysRevE.95.012609>.
- [29] K.E. Achyuthan, J.C. Harper, R.P. Manginell, M.W. Moorman, Volatile metabolites emission by *in vivo* microalgae – an overlooked opportunity? *Metabolites* 7 (2017) 39, <https://doi.org/10.3390/metabo7030039>.
- [30] O.A. Soboleva, P.V. Protchenko, V.V. Korolev, I. Viktorova, A. Yakushenko, R. Kudia, J.S. Gutmann, L.A. Tsarkova, Aroma molecules and dynamic volatile surfactants: functionality beyond the scent, *ACS Appl. Mater. Interfaces* 11 (2019) 40988–40995, <https://doi.org/10.1021/acsami.9b15596>.
- [31] N. Kanei, T. Harigai, H. Kunieda, Effect of added fragrances on the foaming properties of aqueous surfactant solutions, *Int. J. Cosmet. Sci.* 27 (2005) 351–352, <https://doi.org/10.1111/j.1467-2494.2005.00288.3.x>.
- [32] N. Denkov, S. Tcholakova, N. Politova-Brinkova, Physicochemical control of foam properties, *Curr. Opin. Colloid Interface Sci.* 50 (2020) 101376, <https://doi.org/10.1016/j.cocis.2020.08.001>.
- [33] N. Qi, H. Sun, H. Zhao, Y. Li, Achieving foaming control smartly: pre-solubilized flavor oil serves as an *in situ* homogeneous defoamer, *Soft Matter* 14 (2018) 2059–2067, <https://doi.org/10.1039/C7SM02266B>.
- [34] W. Fieber, A. Scheklauk, W. Kunz, M. Pleines, D. Benczedi, T. Zemb, Towards a general understanding of the effects of hydrophobic additives on the viscosity of surfactant solutions, *J. Mol. Liq.* 329 (2021) 115523, <https://doi.org/10.1016/j.molliq.2021.115523>.
- [35] S.E. Friberg, P.A. Aikens, Constant vapor pressure emulsions evaporation: linalool/water stabilized by Laureth 4, *J. Colloid Interface Sci.* 333 (2009) 599–604, <https://doi.org/10.1016/j.jcis.2009.02.034>.
- [36] N. Qi, Z. Chen, H. Zhao, Q. Wang, H. Chen, H. Yuan, Y. Li, Predicting and controlling the effect of solubilized flavor oil on foam properties of surfactant through study of the adsorption activity and configuration, *J. Surfactants Deterg.* 23 (2020) 347–358, <https://doi.org/10.1002/jsde.12364>.
- [37] W. Fieber, S. Frank, C. Herrero, Competition between surfactants and apolar fragrances in micelle cores, *Colloids Surf., A* 539 (2018) 310–318, <https://doi.org/10.1016/j.colsurfa.2017.12.031>.
- [38] A. Parker, W. Fieber, Viscoelasticity of anionic wormlike micelles: effects of ionic strength and small hydrophobic molecules, *Soft Matter* 9 (2013) 1203–1213, <https://doi.org/10.1039/C2SM27078A>.
- [39] G.S. Georgieva, S.E. Anachkov, I. Lieberwirth, K. Koynov, P.A. Kralchevsky, Synergistic growth of giant wormlike micelles in ternary mixed surfactant solutions: effect of octanoic acid, *Langmuir* 32 (2016) 12885–12893, <https://doi.org/10.1021/acs.langmuir.6b03955>.
- [40] S.E. Anachkov, G.S. Georgieva, L. Abezgauz, D. Danino, P.A. Kralchevsky, Viscosity peak due to shape transition from wormlike to disklike micelles: effect of dodecanoic acid, *Langmuir* 34 (2018) 4897–4907, <https://doi.org/10.1021/acs.langmuir.8b00421>.
- [41] S.N. Prasad, M. Muralidhara, Analysis of the antioxidant activity of geraniol employing various *in-vitro* models: relevance to neurodegeneration in diabetic neuropathy, *Asian J. Pharmaceut. Clin. Res.* 10 (2017) 101–105, <https://doi.org/10.22159/ajpcr.2017.v10i7.18564>.
- [42] R. de Cássia da Silveira, L.N. Andrade, D.P. de Sousa, A review on anti-inflammatory activity of monoterpenes, *Molecules* 18 (2013) 1227–1254, <https://doi.org/10.3390/molecules18011227>.
- [43] F. Solórzano-Santos, M.G. Miranda-Novales, Essential oils from aromatic herbs as antimicrobial agents, *Curr. Opin. Biotechnol.* 23 (2012) 136–141, <https://doi.org/10.1016/j.copbio.2011.08.005>.

- [44] S. Carnesecchi, R. Bras-Gonçalves, A. Bradaia, M. Zeisel, F. Gossé, M.F. Poupon, F. Raul, Geraniol, a component of plant essential oils, modulates DNA synthesis and potentiates 5-fluorouracil efficacy on human colon tumor xenografts, *Cancer Lett.* 215 (2004) 53–59, <https://doi.org/10.1016/j.canlet.2004.06.019>.
- [45] B.F. Andrade, C.P. Braga, K.C. Dos Santos, L.N. Barbosa, V.L. Rall, J.M. Sforcin, A. A. Fernandes, A. Fernandes Júnior, Effect of inhaling Cymbopogon martinii essential oil and geraniol on serum biochemistry parameters and oxidative stress in rats, *Biochem. Res. Int.* 2014 (2014) 493183, <https://doi.org/10.1155/2014/493183>.
- [46] C. Gentry, N. Stoakley, D.A. Andersson, S. Bevan, The roles of iPLA2, TRPM8 and TRPA1 in chemically induced cold hypersensitivity, *Mol. Pain* 6 (2010) 4, <https://doi.org/10.1186/1744-8069-6-4>.
- [47] D.D. McKemy, W.M. Neuhäusser, D. Julius, Identification of a cold receptor reveals a general role for TRP channels in thermosensation, *Nature* 416 (2002) 52–58, <https://doi.org/10.1038/nature719>.
- [48] A.M. Peier, A. Moqrich, A.C. Hergarden, A.J. Reeve, D.A. Andersson, G.M. Story, T. J. Earley, I. Dragoni, P. McIntyre, S. Bevan, A. Patapoutian, A TRP channel that senses cold stimuli and menthol, *Cell* 108 (2002) 705–715, [https://doi.org/10.1016/s0092-8674\(02\)00652-9](https://doi.org/10.1016/s0092-8674(02)00652-9).
- [49] T. Limpanuparb, W. Lorpaiboon, K. Chinsukserm, An in silico investigation of menthol metabolism, *PLoS One* 14 (2019) e0216577, <https://doi.org/10.1371/journal.pone.0216577>.
- [50] T.H.D. Nguyen, S.G. Itoh, H. Okumura, M. Tominaga, Structural basis for promiscuous action of monoterpenes on TRP channels, *Commun. Biol.* 4 (2021) 293, <https://doi.org/10.1038/s42003-021-01776-0>.
- [51] Y. Karashima, N. Damann, J. Prenen, K. Talavera, A. Segal, T. Voets, B. Nilius, Bimodal action of menthol on the transient receptor potential channel TRPA1, *J. Neurosci.* 27 (2007) 9874–9884, <https://doi.org/10.1523/jneurosci.2221-07.2007>.
- [52] B. Xiao, A.E. Dubin, B. Bursulaya, V. Viswanath, T.J. Jegla, A. Patapoutian, Identification of transmembrane domain 5 as a critical molecular determinant of menthol sensitivity in mammalian TRPA1 channels, *J. Neurosci.* 28 (2008) 9640–9651, <https://doi.org/10.1523/jneurosci.2772-08.2008>.
- [53] T. Miyamoto, M.J. Petrus, A.E. Dubin, A. Patapoutian, TRPV3 regulates nitric oxide synthase-independent nitric oxide synthesis in the skin, *Nat. Commun.* 2 (2011) 369, <https://doi.org/10.1038/ncomms1371>.
- [54] R. Aijima, B. Wang, T. Takao, H. Mihara, M. Kashio, Y. Ohsaki, J.Q. Zhang, A. Mizuno, M. Suzuki, Y. Yamashita, S. Masuko, M. Goto, M. Tominaga, M.A. Kido, The thermosensitive TRPV3 channel contributes to rapid wound healing in oral epithelia, *FASEB J.* 29 (2015) 182–192, <https://doi.org/10.1096/fj.14-251314>.
- [55] G.P.P. Kamatou, I. Vermaak, A.M. Viljoen, B.M. Lawrence, Menthol: a simple monoterpene with remarkable biological properties, *Phytochemistry* 96 (2013) 15–25, <https://doi.org/10.1016/j.phytochem.2013.08.005>.
- [56] G. Işcan, N. Kirimer, M. Kürkcüoğlu, K.H. Başer, F. Demirci, Antimicrobial screening of *Mentha piperita* essential oils, *J. Agric. Food Chem.* 50 (2002) 3943–3946, <https://doi.org/10.1021/jf011476k>.
- [57] E.A. Laude, A.H. Morice, T.J. Grattan, The antitussive effects of menthol, camphor and cineole in conscious Guinea-pigs, *Pulm. Pharmacologist* 7 (1994) 179–184, <https://doi.org/10.1006/pulp.1994.1021>.
- [58] J. Tamaoki, A. Chiyotani, A. Sakai, H. Takemura, K. Konno, Effect of menthol vapor on airway hyperresponsiveness in patients with mild asthma, *Respir. Med.* 89 (1995) 503–504, [https://doi.org/10.1016/0954-6111\(95\)90127-2](https://doi.org/10.1016/0954-6111(95)90127-2).
- [59] B.G. Green, B.L. McAuliffe, Menthol desensitization of capsaicin irritation. Evidence of a short-term anti-nociceptive effect, *Physiol. Behav.* 68 (2000) 631–639, [https://doi.org/10.1016/s0031-9384\(99\)00221-8](https://doi.org/10.1016/s0031-9384(99)00221-8).
- [60] M.A. Teixeira, O. Rodríguez, V.G. Mata, A.E. Rodrigues, The diffusion of perfume mixtures and the odor performance, *Chem. Eng. Sci.* 64 (2009) 2570–2589, <https://doi.org/10.1016/j.ces.2009.01.064>.
- [61] M.A. Teixeira, O. Rodríguez, A.E. Rodrigues, Diffusion and performance of fragranced products: prediction and validation, *AIChE J.* 59 (2013) 3943–3957, <https://doi.org/10.1002/aic.14106>.
- [62] N.C. Christov, K.D. Danov, P.A. Kralchevsky, K.P. Ananthapadmanabhan, A. Lips, Maximum bubble pressure method: universal surface age and transport mechanism in surfactant solutions, *Langmuir* 22 (2006) 7528–7542, <https://doi.org/10.1021/la061239h>.
- [63] K.D. Danov, R.D. Stanimirova, P.A. Kralchevsky, K.G. Marinova, N.A. Alexandrov, S.D. Stoyanov, T.B.J. Blijdenstein, E.G. Pelan, Capillary meniscus dynamometry – method for determining the surface tension of drops and bubbles with isotropic and anisotropic surface stress distributions, *J. Colloid Interface Sci.* 440 (2015) 168–178, <https://doi.org/10.1016/j.jcis.2014.10.067>.
- [64] K.D. Danov, P.A. Kralchevsky, K.P. Ananthapadmanabhan, A. Lips, Interpretation of surface-tension isotherms of *n*-alkanoic (fatty) acids by means of the van der Waals model, *J. Colloid Interface Sci.* 300 (2006) 809–813, <https://doi.org/10.1016/j.jcis.2006.04.026>.
- [65] E.H. Lucassen-Reynders, A. Cagna, J. Lucassen, Gibbs elasticity, surface dilatational modulus and diffusional relaxation in nonionic surfactant monolayers, *Colloids Surf., A* 186 (2001) 63–72, [https://doi.org/10.1016/S0927-7757\(01\)00483-6](https://doi.org/10.1016/S0927-7757(01)00483-6).
- [66] J.F. Baret, Theoretical model for an interface allowing a kinetic study of adsorption, *J. Colloid Interface Sci.* 30 (1969) 1–12, [https://doi.org/10.1016/0021-9797\(69\)90373-7](https://doi.org/10.1016/0021-9797(69)90373-7).
- [67] P.A. Kralchevsky, K.D. Danov, V.L. Kolev, G. Broze, A. Mehreteab, Effect of nonionic admixtures on the adsorption of ionic surfactants at fluid interfaces. 1. Sodium dodecyl sulfate and dodecanol, *Langmuir* 19 (2003) 5004–5018, <https://doi.org/10.1021/la0268496>.
- [68] C.M. Phan, The surface tension and interfacial composition of water/ethanol mixture, *J. Mol. Liq.* 342 (2021) 117505, <https://doi.org/10.1016/j.molliq.2021.117505>.
- [69] J. Yu, Z. Pan, Non-selective evaporation of ethanol-water binary mixture within heated capillary, *Int. Commun. Heat Mass Tran.* 159 (2024) 108174, <https://doi.org/10.1016/j.icheatmasstransfer.2024.108174>.